A Plant-inspired Light Transducer for High-performance Near-infrared Light Mediated Gas Sensing

Liang, Hongping; Guo, Xin; Guo, Lanpeng; Liu, Siying; Zhan, Qiuqiang; Yang, Haihong; Li, Hao; de Rooij, Nicolaas Frans; Lee, Yi Kuen; French, Paddy J.

DOI
10.1002/adfm.202215099

Publication date
2023

Document Version
Final published version

Published in
Advanced Functional Materials

Citation (APA)
Liang, H., Guo, X., Guo, L., Liu, S., Zhan, Q., Yang, H., Li, H., de Rooij, N. F., Lee, Y. K., French, P. J., Wang, Y., & Zhou, G. (2023). A Plant-inspired Light Transducer for High-performance Near-infrared Light Mediated Gas Sensing. *Advanced Functional Materials*, *33*(21), Article 2215099. https://doi.org/10.1002/adfm.202215099

ADVANCED FUNCTIONAL MATERIALS
www.afm-journal.de

A Plant-inspired Light Transducer for High-performance Near-infrared Light Mediated Gas Sensing

Hongping Liang, Xin Guo, Lanpeng Guo, Siying Liu, Qiuqiang Zhan, Haihong Yang, Hao Li, Nicolaas Frans de Rooij, Yi-Kuen Lee, Paddy J. French, Yao Wang, and Guofu Zhou*

Constructing near-infrared light (NIR) light-enhanced room temperature gas sensors is becoming more promising for practical application. In this study, learning from the structure and photosynthetic process of chlorophyll thylakoid membranes in plants, the first "Thylakoid membrane" structural formaldehyde (HCHO) sensor is constructed by matching the upconversion emission of the lanthanide-doped upconversion nanoparticles (UCNPs) and the UV–vis adsorption of the as-prepared nanocomposites. The NIR-mediated sensor exhibits excellent performances, including ultra-high response (R_a / R_g = 2.22, 1 ppm), low practical limit of detection (50 ppb), reliable repeatability, high selectivity, and broadband spectral response. The practicality of the NIR-mediated gas sensor is confirmed through the remote and external stimulation test. A study of sensing mechanism demonstrates that it is the UCNPs-based light transducer produces more light-induced oxygen species for gas response in the process of non-radiative/radiative energy transfer, playing a key role in significantly improving the sensing properties of the sensor. The universality of NIR-mediated gas sensors based on UCNPs is verified using ZnO, In_2O_3, and SnO_2 systems. This work paves a way for fabricating high-performance NIR-mediated gas sensors and will expand the application fields of NIR light.

1. Introduction

The utilization of infrared (IR) including near-, mid-, and far-infrared light has been pursued by scientists in many fields since its proportion in natural sunlight is nearly 50%.[1,2] Compared with UV–vis light, near-infrared (NIR) light as the highest energy part of IR has the advantage of relatively lower energy consumption, larger penetration depth, and less harmful, which makes it ideal for practical applications in the realms of imaging,[3] photocatalysis[4] and sensing,[5–7] etc. Especially, multiple gases can be distinguished and detected using gas sensors with the enhancement of a single nondispersive NIR light source, which enables it promising to build a low-power single-chip sensing microsystem.[8–10] Until now, it is reported that only a few compounds with narrow bandgap could absorb NIR light to obtain the required activation energy for gas sensing.[11] For example, Wang et al.[7] functionalized ZnO nanorods with narrow bandgap (0.41 eV) PbS quantum dots (PbS QDs) enabling the electron transfer from PbS QDs to ZnO under NIR illumination, successfully improving the room temperature NO_2 response of the sensor. Nevertheless, for most of gas sensing materials, high activation energy is required because of their wide bandgap, which is obviously excessive for relatively low-energy NIR light.[12–14] Therefore, developing a universal NIR-mediated gas sensing strategy will open a new prospect for the development of room temperature gas sensors. To the best of our knowledge, a universal strategy to construct a NIR-mediated ultrasensitive room temperature gas sensor has not been reported.

H. Liang, X. Guo, L. Guo, S. Liu, Q. Zhan, H. Li, Y. Wang, G. Zhou
Guangdong Provincial Key Laboratory of Optical Information Materials and Technology
Institute of Electronic Paper Displays
South China Academy of Advanced Optoelectronics
South China Normal University
Guangzhou 510006, P.R. China
E-mail: wangyao@m.scnu.edu.cn

H. Liang, L. Guo, H. Li, N. F. de Rooij, Y. Wang, G. Zhou
National Center for International Research on Green Optoelectronics
South China Normal University
Guangzhou 510006, P.R. China

The ORCID identification number(s) for the author(s) of this article can be found under https://doi.org/10.1002/adfm.202215099.

DOI: 10.1002/adfm.202215099

H. Liang
School of Electronic Information and Electrical Engineering
Huizhou University
Huizhou 516007, P.R. China

H. Yang
Department of Thoracic Oncology
State Key Laboratory of Respiratory Diseases
The First Affiliated Hospital of Guangzhou Medical University
Guangzhou 510006, P.R. China

Y.-K. Lee
Department of Mechanical and Aerospace Engineering
Department of Electronic and Computer Engineering
Hong Kong University of Science and Technology
Clear Water Bay, Kowloon, Hong Kong SAR 999077, China

P. J. French
EEMCS
Delft University of Technology
Delft 2628 CD, The Netherlands

Chlorophyll thylakoid membrane is the reaction platform in photosynthesis of plants, which is composed of "light transducer", "electron transporter" and "reaction center".[15] Under irradiation, the "light transducer" in the thylakoid membrane receives light energy and transfers it to the "reaction center" through the "electron transporter". So, full-spectrum sunlight is able to be quickly and effectively converted into electrical and chemical energy through a redox process inside plants. The special structure and photosynthetic mechanism of thylakoid membrane drive us to think, whether or not we could construct an artificial "light transducer" to absorb NIR light for gas sensing? Based on our previous works,[16] ZnO could behave the best room temperature formaldehyde (HCHO) sensing performance under UV–vis light. Light photoactivation is widely used to improve room temperature gas sensing performance, especially for formaldehyde (HCHO), a harmful indoor pollutant[10] and vital biomarker.[17] A light transducer that could convert NIR to UV–vis matching the absorption of ZnO should be the key to the "door". Meanwhile, it is known that lanthanide-doped upconversion nanoparticles (UCNPs) possess an anti-Stokes nature of converting low-energy NIR light to high-energy UV–vis light efficiently.[18–20] Thereby, combining the above two aspects of foundation, the first "Thylakoid membrane" like room temperature HCHO sensor could be designed by matching the upconversion emission of the UCNPs and the UV–vis adsorption of the sensing materials.[21]

In this work, learning from the structure and photosynthetic process of chlorophyll thylakoid membranes in plants, we have constructed the first NIR-mediated HCHO sensor with a thylakoid membrane-like structure. The fabricated NIR-mediated sensor is composed of the "light transducer" made from the polyelectrolyte-coated UCNPs, the "electron transporter" formed from the dipole-modified graphene nanosheets and the "reaction center" derived from the nanocomposites of graphene and zinc oxide. The obtained sensor exhibits excellent performances, including ultra-high response, low practical limit of detection, reliable repeatability, high selectivity, and broadband spectral response. The improved NIR-mediated gas sensing performance can also be obtained with In_2O_3 and SnO_2 under the functionalization of UCNPs, verifying the universality of this strategy.[22] This design paves a way for the construction of high-performance NIR-mediated gas sensing platforms for gas monitoring.

2. Results and Discussion

2.1. Design of "Thylakoid Membrane" Structural Sensor

A facile and universal NIR-mediated gas sensing strategy is proposed by constructing the "Thylakoid membrane" structure. The schematic illustration of the as-proposed "Thylakoid membrane" structural sensor and the related mechanism was shown in **Figure 1**. First, oleic acid (OA)-coated UCNPs are successfully prepared by a thermal decomposition method, and the poly (sodium p-styrenesulfonate) coated UCNPs (PSS@UCNPs) are successfully prepared by coating a thin PSS layer through a ligand-free method.[23] Second, the 5-aminonaphthalene-1-sulfonic acid-functionalized graphene (ANS-rGO) and the

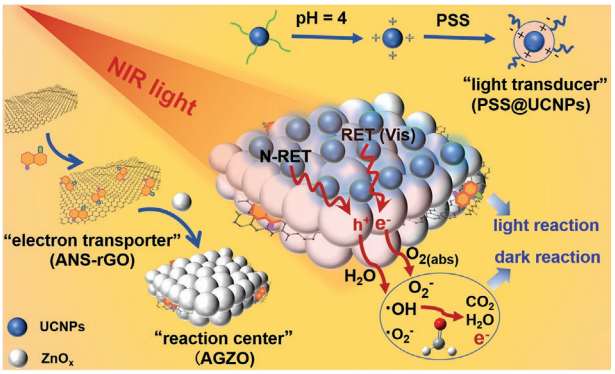

Figure 1. Schematic illustrations of the as-proposed "Thylakoid membrane" structural sensor.

ANS-rGO/zinc oxide nanocomposites (AGZO) nanocomposites are synthesized by our previous technology.[16] Here, the PSS@UCNPs act as "light transducer" and the ANS-rGO is used as "electron transporter" to improve the light collecting efficiency and provide more electrons to the "reaction center" to activate the sensing process under NIR (980 nm) light illumination. There are three crucial factors in this design to be highlighted: i) The PSS@UCNPs serve as "light transducer" that could convert NIR (980 nm) light into UV–vis light. ii) The NIR light could activate the reactive oxygen species (ROS) with high HCHO catalytic activity. iii) The AGZO act as "reaction center" could absorb the UV–vis light to produce photogenerated electrons and finally more light-induced oxygen species. Here, the PSS layer can prevent the thermal vibrational phonon exchange between UCNPs and AGZO.

2.2. Synthesis and Characterization of ANS-rGO, UCNPs, and AGZO/PSS@Tm

As evidenced by Figure S1, (Supporting Information), the thickness of ANS-rGO (4 nm) is maintained the same as the GO (4 nm), which is much thinner than that of rGO (20–28 nm). In order to broaden the wavelength range of visible light emission, two kinds of UCNPs with the upconversion emission band covering the whole visible light region were synthesized. As shown in Figure S2a,b, (Supporting Information), the as-synthesized OA-coated $NaYF_4$: Yb/Er (30/2%) (OA@Er) exhibit uniform and well-dispersed spherical morphologies with a diameter of a≈22.8 nm, while the PSS-coated Er-UCNPs (PSS@Er) possess ≈ 5 nm layers. The lattice fringes with a spacing of ≈ 0.52 nm and 0.29 nm corresponding to the (100) and (110) planes are observed (Figure S2c, Supporting Information). The Er-UCNPs exhibited green/red upconversion luminescence under 980 nm excitation (Figure S2d, Supporting Information), with emission peaks located at 531–563 nm ($^4S_{3/2}\rightarrow{}^4I_{15/2}$) and 633–685 nm ($^4F_{9/2}\rightarrow{}^4I_{15/2}$).[24] The OA-coated $NaYF_4$: Yb/Tm (50/2%) (OA@Tm) exhibit uniform and well-dispersed spherical morphologies with an average diameter of 53.6 nm (Figure S4a,b, Supporting Information), while the PSS-coated Tm-UCNPs (PSS@Tm) possess ≈ 2.8 nm layers (**Figure 2**b; Figure S3a,b, Supporting Information) with an average diameter of 56.4 nm (Figure S4c,d, Supporting Information). Also, lattice fringes

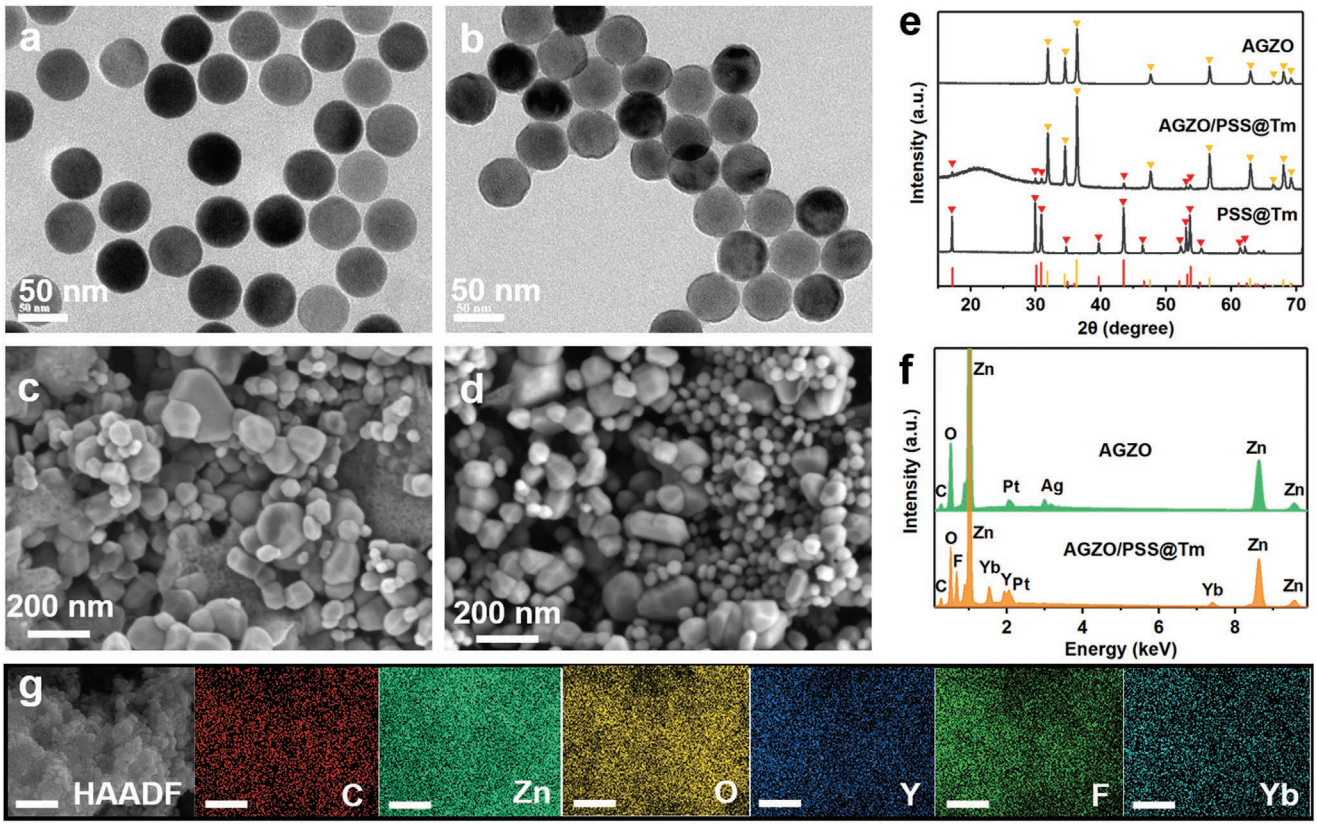

Figure 2. TEM images of a) OA-coated $NaYF_4$: Yb/Tm (50/2%) UCNPs and b) PSS-coated Tm-UCNPs. SEM images of c) AGZO and d) AGZO/PSS@Tm. e) XRD patterns of the PSS@Tm, AGZO and AGZO/PSS@Tm. Hexagonal $NaYF_4$, red color (JCPDF#00-016-0334), hexagonal wurtzite ZnO, yellow color (JCPDS#36-1451). f) EDS spectrum and g) elemental mapping of AGZO/PSS@Tm.

with a spacing of ≈ 0.53 nm in accordance with the (100) plane of Tm-UCNPs were observed (Figure S3c, Supporting Information). As shown in Figure S3d, (Supporting Information), the upconversion fluorescence emission of Tm-UCNPs can be split into a blue region of 450 nm ($^1D_2 \rightarrow {}^3F_4$) and 475 nm ($^1G_4 \rightarrow {}^3H_6$) and a red region of 645 nm ($^1G_4 \rightarrow {}^3F_4$). Figure S5, Supporting Information shows that PSS-coated UCNPs were rich in PSS carbon skeleton groups, which suggests the successful coating of PSS on UCNPs. The peaks are assigned as follows: i) S=O stretching vibration (1656 cm^{-1}), ii) benzene ring absorption (1412 cm^{-1}), iii) C−C vibration band (1186–1130 cm^{-1}). Importantly, similar upconversion luminescence intensities can be observed at the same dispersion concentration between OA@Tm and PSS@Tm (Figure S6, Supporting Information), indicating the importance of PSS coating for maintaining luminescence efficiency. As a comparison, the upconversion luminescence intensity of ligand-free Tm-UCNPs decreases greatly due to the surface quenching effect. The steady upconversion luminescence shows that the as-prepared UCNPs can be used as efficient energy donors.

As demonstrated in Figure 2c,d, SEM images reveal that the UCNPs were well-distributed on the AGZO which provides a good foundation for constructing the "Thylakoid membrane" structure. It is quite clear that a uniform surface morphology over a broad range of AGZO/PSS@Tm areas on the IDEs can be formed (Figure S7, Supporting Information). XRD results in Figure 2e showed that the AGZO/PSS@Tm contained both hexagonal wurtzite ZnO and hexagonal $NaYF_4$ crystals according to the standard data (JCPDS#36-1451, JCPDS# 00-016-0334).[25,26] To further prove the successful spin coating of PSS@Tm on AGZO, the EDS spectrum (Figure 2f) and the elemental mapping (Figure 2g) were measured, revealing that AGZO/PSS@Tm is mainly composed of C, Zn, O, Y, F, and Yb.

2.3. Feasibility of NIR-mediated Gas Sensing Strategy

Imitating the "Thylakoid membrane" structure, UCNPs were utilized as the light transducer to convert NIR light into visible light that could be captured by the AGZO (reaction center). The feasibility of the proposed NIR-mediated gas sensing strategy was verified through the absorption and emission characteristics of UCNPs before and after being assembled with AGZO. As we know, a sensitizer (Yb^{3+}) could sensitize the activator (Tm^{3+}) under 980 nm excitation. As shown in **Figure 3**a, the blue emission peaks at 450 nm and 475 nm, as well as the red emission peaks at 645 nm are assigned to the $^1D_2 \rightarrow {}^3F_4$, $^1G_4 \rightarrow {}^3H_6$ and $^1G_4 \rightarrow {}^3F_4$ transitions (energy transfer) of Tm^{3+} ions, respectively, which basically consistent with that of other literature.[20,27,28] To further confirm the effective energy transfer between PSS@Tm and AGZO, the absorption characteristics of the AGZO sensing materials and the PSS@Tm were examined by UV–vis

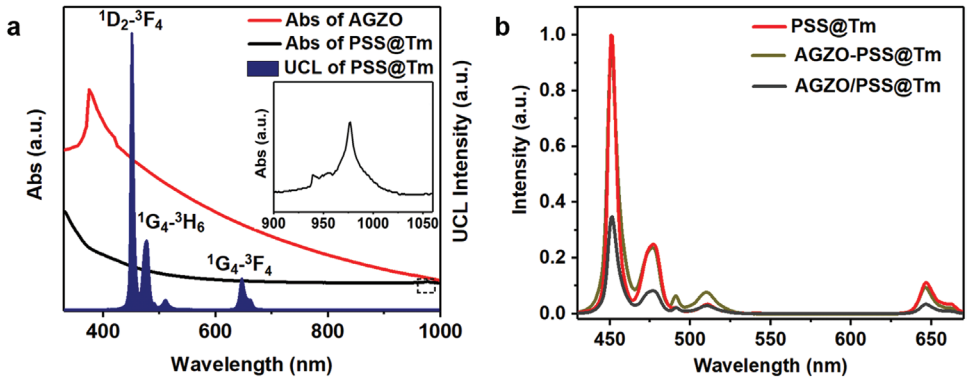

Figure 3. a) UV–vis absorption spectra of PSS@Tm (black curve) and AGZO (red curve). The blue curve showed the fluorescence spectrum of PSS@Tm. b) Fluorescence spectra of PSS@Tm, AGZO/PSS@Tm and AGZO-PSS@Tm mixture under 980 nm excitation at room temperature.

spectroscopy. As shown in Figure 3a. The reference PSS@Tm shows absorption peaks near 980 nm (inset) and the UV region. The UV–vis spectrum of AGZO reveals a strong absorption band at 380–500 nm owing to its rich oxygen vacancy defects.[16] Interestingly, the PSS@Tm displays an obvious upconversion luminescence (UCL) emission band in the 440–500 nm region, which overlaps well with the UV–vis absorption region of AGZO sensing materials. The overlap of the UV–vis absorption region of AGZO and the UCL emission region of PSS@Tm proves the efficient energy transfer from PSS@Tm to AGZO.[29] These results indicated that the AGZO sensing materials can be activated by the PSS@Tm through the energy transfer between them to realize NIR-mediated gas sensing. As shown in Figure 3b and Table S1, the integrated UCL intensity of PSS@Tm decreases after being combined with the AGZO sensing layer, indicating that AGZO can absorb the UCL of PSS@Tm. Figure S8, Supporting Information shows the photoresponse curves of the AGZO and AGZO/PSS@Tm-1:50 based sensors to 980 nm illumination under a bias potential of 20 V. The visible light emitted by the PSS@Tm was absorbed by AGZO, resulting in the separation of electrons and holes. As shown in Figure S8a, Supporting Information, the current of AGZO reduce from 96 nA to 64 nA after 980 nm irradiation, which may be due to the activation of adsorbent (O_2, H_2O, etc.) on the surface of the material under NIR light.[30–32] For n-type semiconductors (electrons are the majority charge carriers), an electron depletion layer is formed in the interface area of AGZO after the electrons are captured by the adsorbent to form ROS, reducing the conductivity of the material.[29] After AGZO was assembled with PSS@Tm, the current of AGZO/PSS@Tm-1:50 increased by 3.3 nA under 980 nm irradiation (Figure S8b, Supporting Information). This phenomenon confirms that NIR input is successfully converted into photocurrent output with the help of AGZO/PSS@Tm.

2.4. Gas Sensing Performances of Sensors

We explored the optimal conditions for obtaining high sensing performances. The sensing properties of AGZO/PSS@Tm were first optimized by controlling the dilution ratio of PSS@Tm. With the decreased dilution ratio, the response value showed a tendency from increasing to decreasing (**Figure 4**a) because of the severe cover of AGZO by PSS@Tm, which results in the decreased reaction site on the surface of sensing materials reacting with HCHO. The sensing properties of the AGZO and AGZO/PSS@Tm-1:50 based sensors toward 0.2 ppm of HCHO with/without 980 nm (60 $mW \cdot cm^{-2}$) illumination were also studied. As shown in Figure 4b, the AGZO-based sensor displayed a response value of 1.15 toward 0.2 ppm HCHO, which may be due to the formation of NIR-induced reactive oxygen species on the sensing materials surface under 980 nm illumination. After functionalization with PSS@Tm, the AGZO/PSS@Tm-1:50 sensor exhibited an increased response (1.36) and fast response/recovery speed (250 s/250 s). Thus, the enhanced HCHO sensing performances of the AGZO and AGZO/PSS@Tm-1:50 could be observed under NIR illumination. Although a similar trend was also observed on AGZO based sensor, the response value of AGZO/PSS@Tm-1:50 is 2.5 times higher than that of AGZO. Moreover, the light intensity of 980 nm showed little influence on the sensing performance when we increased the light intensity from 30 $mW \cdot cm^{-2}$ to 120 $mW \cdot cm^{-2}$. As shown in Figure 4c, the corresponding response value of AGZO/PSS@Tm-1:50 sensor toward 1ppm HCHO displayed a slight trend from increasing to decreasing under the light intensity of 30 $mW \cdot cm^{-2}$, 60 $mW \cdot cm^{-2}$, 90 $mW \cdot cm^{-2}$ and 120 $mW \cdot cm^{-2}$, which also illustrates the occurrence of effective energy transfer from PSS@Tm to AGZO. As a control group, the sensing performance of AGZO/PSS@Tm-1:50 under the direct irradiation of 450 nm blue light was also measured with the same power intensity of 980 nm NIR light. As shown in Figure 4d, AGZO/PSS@Tm-1:50-based sensor was activated under 450 nm irradiation directly, possessing a much lower sensitivity (R_a / R_g = 1.15) than that of under 980 nm (R_a / R_g = 1.51) irradiation, even though the power of blue light is much higher than the blue luminescence of UCNPs with very low quantum yield.[33]

These results reveal that the improved sensing performances not only originate from the energy transfer between PSS@Tm donor and AGZO acceptor but also from the other factors that should be emphasized. As we know, reactive oxygen species can be produced on the surface of photosensitizers under appropriate light excitation,[34] which can also be directly confirmed by the improvement of sensitivity under high relative humidity (**Figure 5**f). Therefore, the excellent gas

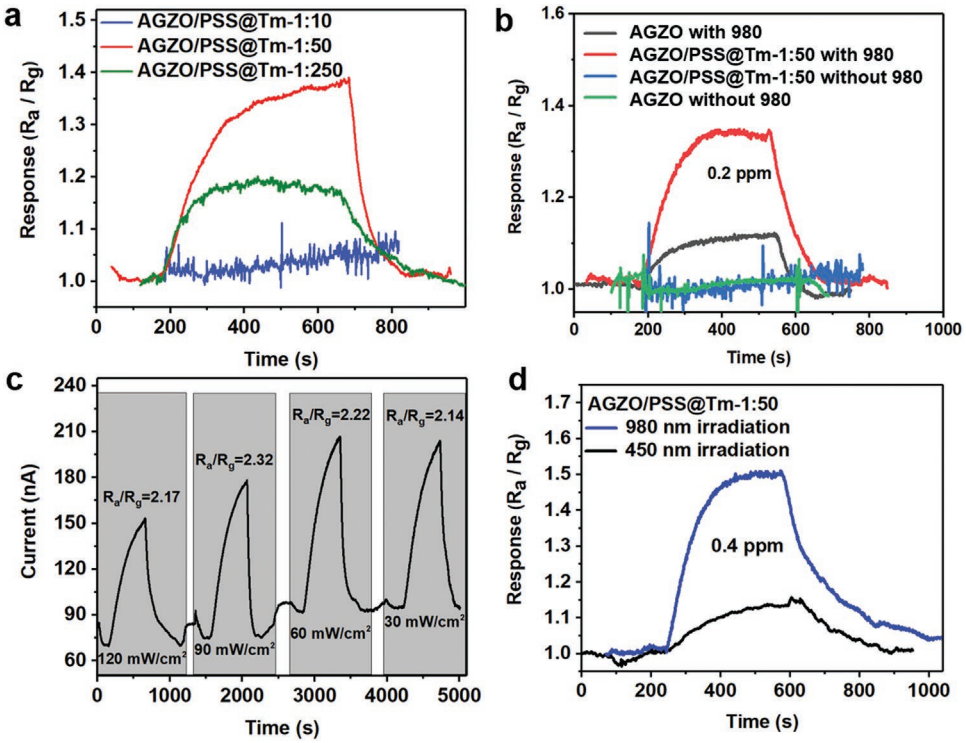

Figure 4. a) The effect of dilution ratio of PSS@Tm on the sensing performance of AGZO/PSS@Tm. b) The effect of PSS@Tm addition on the sensing performance of AGZO with/without 980 nm illumination. c) Typical response curve of the sensor toward 1 ppm HCHO under different 980 nm light intensity. d) Typical response curve of the sensor toward 0.4 ppm HCHO under 450 nm and 980 nm irradiation, respectively.

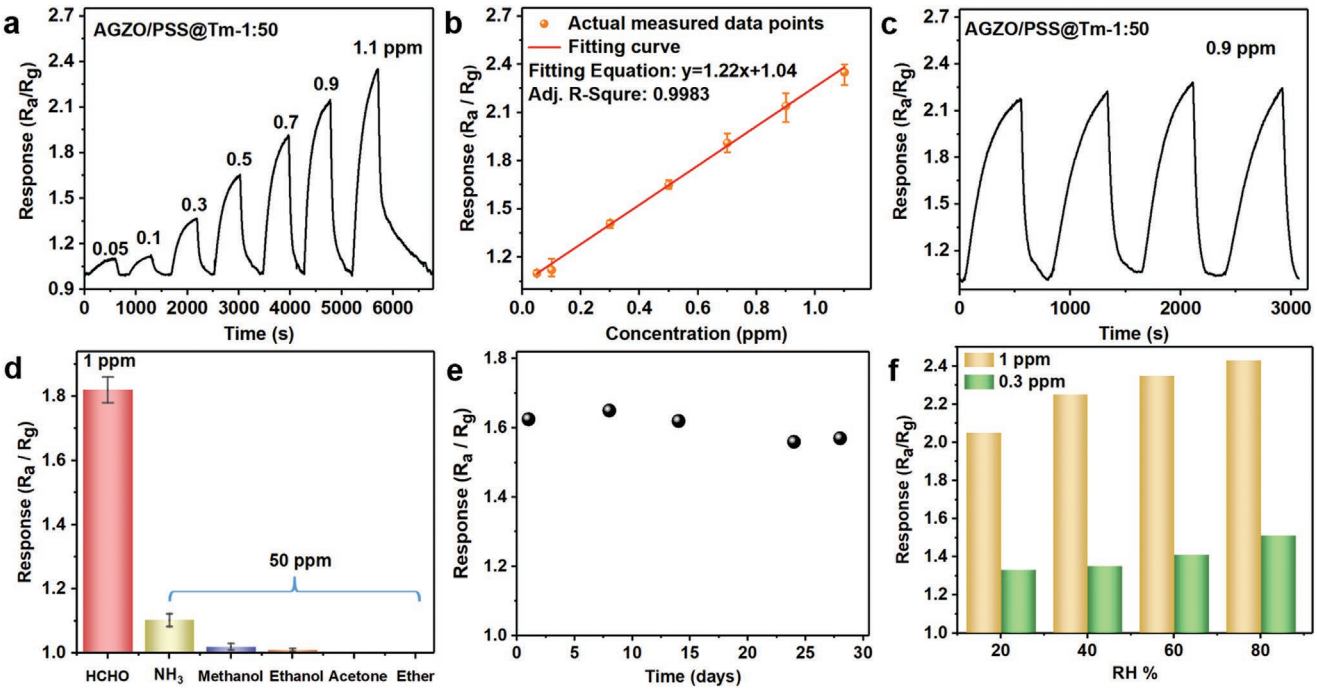

Figure 5. a) Response curves of AGZO/PSS@Tm-1:50 gas sensors upon exposed to 0.05–1.1 ppm HCHO under 980 nm illumination. b) the corresponding fitted curve of the response value. c) Cycling performance of the sensor in response to HCHO at 0.9 ppm. d) Selectivity of the sensor to various gases at 50 ppm. e) Long-term stability of the sensor under 0.5 ppm of HCHO. f) The response of the sensor toward 0.3 ppm and 1 ppm HCHO at varying relative humidity from 20% to 80%.

Table 1. Comparison of the sensing performances for representative room temperature HCHO sensors.

Materials	HCHO	Light [@RT]	Response	LOD [ppm]
Ni–In_2O_3/WS_2[35]	20 ppm	no light	1.47^{ε}	0.05
ZnO-ANS-rGO[36]	5 ppm	no light	1.05^{δ}	5
cactus-like ZnO/ANS-rGO[37]	5 ppm	no light	1.68^{δ}	0.25
In_2O_3/PW_{12}[38]	100 ppm	Xe lamp	1.82^{ε}	5
POM@ZIF-8@ZnO[39]	100 ppm	Xe lamp	5.4^{ε}	25
MOF-ZnO[40]	1 ppm	365 nm	$\sim 2^{\varepsilon}$	0.1
5MMM/TiO_2[41]	5 ppm	365 nm	1350^{ε}	0.025
ZnO_x@ANS-rGO[16]	1 ppm	405 nm	1.58^{ε}	0.005
AGZO/PSS@Tm (This work)	1 ppm	980 nm	2.22^{ε}	0.05

Room temperature (RT), Limit of detection (LOD). For the convenience of comparison, the evaluation of Response was converted as ε: Response = R_a/R_g, δ: Response = R_g/R_a.

sensing properties of AGZO/PSS@Tm-1:50 can be reasonably attributed to two facts: i) NIR-triggered reactive oxygen species (ROS) with high catalytic activity can be formed on the surface of AGZO; ii) PSS@Tm supply AGZO with blue light (440–500 nm) through non-radiative/radiative energy transfer (N/RET) process after absorbing NIR light. Under 980 nm irradiation, AGZO can be activated only by ROS produced on its surface. After assembly with PSS@Tm, both ROS and the N/RET process will occur.

The response-recovery curves and the corresponding fitting curves of the AGZO/ PSS@Tm-1:50-based sensor exposed to 0.05–1.1 ppm HCHO under 980 nm illumination are summarized in Figure 5a,b. Through linear fitting between the response value and formaldehyde concentration, excellent linear dependence (R^2 = 0.9983) and sensitivity (1.22/ppm) were demonstrated. A comparison of the sensing performances for the representative room-temperature HCHO sensors in the literature is displayed in **Table 1**. To reveal its repeatability, four response–recovery cycles of the AGZO/PSS@Tm-1:50 sensor to 0.9 ppm of HCHO under 980 nm irradiation were performed. Stable responses of 2.11–2.23 demonstrated the good repeatability and recoverability of the sensor (Figure 5c). In order to prove that the sensor has a good selectivity even in the NIR illumination, the responses of the AGZO/PSS@Tm-1:50 sensor to 1 ppm of HCHO and 50 ppm of other hazardous gases (ammonia, methanol, ethanol, ether, and acetone) under NIR illumination were also performed. The results show that the NIR-mediated AGZO/PSS@Tm-1:50 sensor exhibited high selectivity to HCHO, indicating that it can be used for HCHO detection (Figure 5d). Figure 5e shows the long-term stability of the AGZO/PSS@Tm-1:50 sensor. The response of the AGZO/PSS@Tm-1:50 sensor toward 0.5 ppm of HCHO decreased slightly with time, a response drift of less than 8% could be seen in 30 days, indicating its stable RT sensing performance under 980 nm irradiation. Furthermore, for practical gas sensing applications, the effect of relative humidity (RH) on the sensing properties of the AGZO/PSS@Tm-1:50 sensor needs to be studied. As shown in Figure 5f, interestingly, the response value of the NIR-mediated AGZO/PSS@Tm-1:50 sensor exhibited an upward trend within the relative humidity range from 20% to 80%. There are two reasons why the response value of HCHO increases with the increase in humidity. On the one hand, it has been reported that the photocatalytic oxidation of water vapor on the material's surface under NIR illumination can generate hydroxyl radical (•OH) through the reaction of $OH^- + h^+$ ($h\nu$) → •OH ($h\nu$).[30–32] Thus, the photocatalytic oxidation of adsorbed water is facilitated to generate •OH to react with HCHO under light illumination in the presence of water vapor (HCHO + •OH ($h\nu$) → CO_2 +H_2O+$2H^+$ + $2e^-$).[12] On the other hand, the graphene conductive platform providing a fast electron transport path for the sensing process in a humid environment can suppress the cross-sensitivity of the sensors to water vapor.[16,42] This work demonstrated a simple and generic approach for humidity-resistance gas sensors by introducing UCNPs coating and a graphene conductive platform.

2.5. Verification of the Large Penetration Depth of NIR Light and the Universality of NIR-mediated Gas Sensor

As shown in **Figure 6**a, the response value of the AGZO/PSS@Tm-1:50 sensor toward 1 ppm HCHO decreases only ≈8% slightly, even though the sensor is 1.5 m away from the 980 nm light source. More importantly, a similar response curve can be observed in Figure 6b for AGZO/PSS@Tm-1:50 sensor under a 980 nm light source at a distance of 1.5 m with a plastic plate covered on the test chamber (Figure S9, Supporting Information). The excellent sensing performances of NIR-mediated sensors should be ascribed to the much higher penetration depth and the less light scattering of NIR light than blue light. The proposed NIR-mediated gas sensing strategy was extended to various metal oxide semiconductors (e.g. In_2O_3 and SnO_2) and Er-doped UCNPs systems. Figure S10, Supporting Information shows the photo-response curves of AGIn/PSS@Tm-1:50-based sensors under 980 nm illumination at room temperature. Based on the effective energy transfer, the current of the AGIn/PSS@Tm-1:50 sensor increases rapidly and then decreases to a relatively stable state under 980 nm irradiation. This phenomenon confirmed that the PSS@Tm has successfully converted NIR into visible light which can be utilized by the gas sensing materials to enhance gas sensing performances. As shown in Figure 6c,d, improved sensing performance can also be observed for AGIn/PSS@Tm-1:50 and AGSn/PSS@Tm-1:50-based sensors, demonstrating that the NIR-mediated sensing strategy is universal in the gas sensors field. Figure S11, Supporting Information shows the response curves of AGIn/PSS@Er-1:50 based sensors toward 1 ppm HCHO under 980 nm illumination at room temperature. These results demonstrate that the conversion of NIR light to UV–vis light through UCNPs is an ideal strategy to inherit the advantages of NIR light and meet the activation energy requirement of traditional gas sensing materials. The capability of external and remote activating of the sensor was demonstrated, suggesting the potential to construct high-performance NIR-mediated gas sensing platforms which may be extended to detect other targets from human tissues.[43]

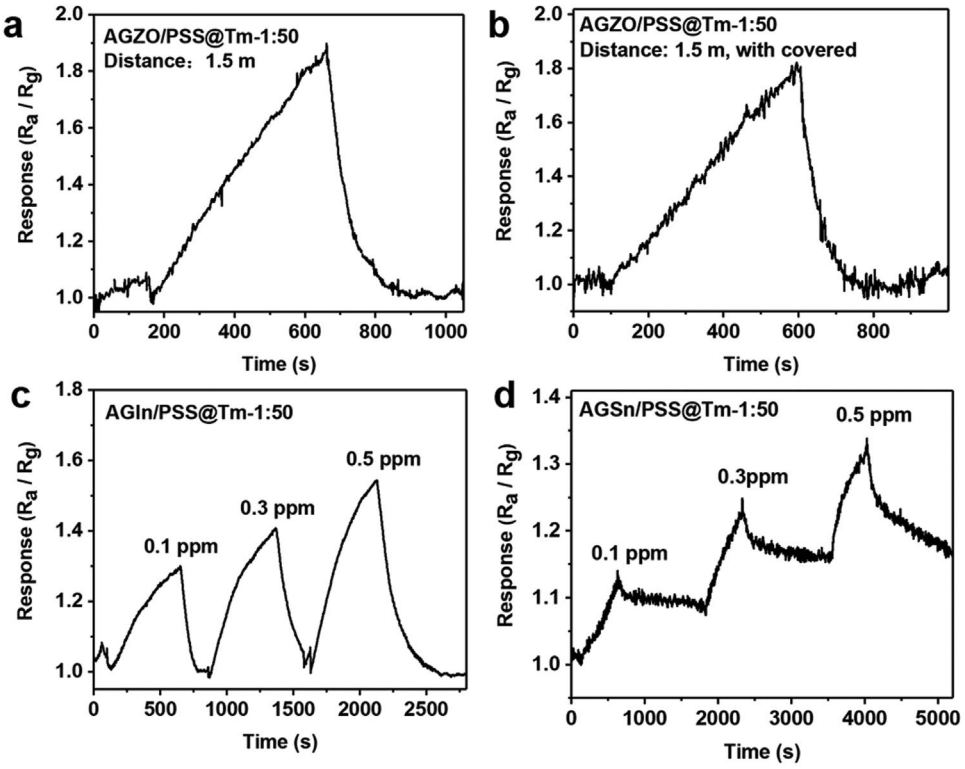

Figure 6. Response curves of AGZO/PSS@Tm-1:50 sensor toward 1 ppm HCHO under 980 nm illumination at a distance of 1.5 m a) without or b) with a plastic plate covered. Response curves of c) AGIn/PSS@Tm-1:50 and d) AGSn/PSS@Tm-1:50-based sensors toward 0.1–0.5 ppm HCHO under 980 nm illumination.

2.6. Gas Sensing Mechanism

The growth mechanism of the UCNPs with high luminescent efficiency has been extensively investigated. In this work, we mainly focus on the energy transfers between UCNPs and gas sensing materials. Actually, energy transfer between UCNPs and metal oxide semiconductors[44,45] or graphene[46] has been widely reported. It should be noted that NIR-mediated gas sensors are reported for the first time in this work. This work provides a new strategy to construct NIR-mediated ultrasensitive gas sensors at room temperature. Moreover, the energy transfer process between UCNPs and sensing materials was proved to be non-radiative/radiative energy transfer (N/RET) by the steady-state and transient fluorescence spectra of PSS@Tm and AGZO/PSS@Tm. On one hand, according to the steady-state spectra in Figure 3b, the reduction in UCL intensity after PSS@Tm spin-coated on AGZO supports that the energy is transferred efficiently from PSS@Tm to AGZO through a radiative energy transfer process. On the other hand, the shortening of UCL lifetime of energy donors is an important signal of non-radiative energy transfer.[47] As observed from Figure S12, (Supporting Information), the UCL decay curves of AGZO/PSS@Tm-1:50 monitored at 450 and 475 nm emission wavelength moved slightly toward a decreased lifetime. As shown in Table S2, the UCL decay time constant lifetime (τ) values of AGZO/PSS@Tm-1:50 at 450 nm ($^1D_2$ level) and 475 nm ($^1G_4$ level) are 0.829 and 5.314 ms, respectively, which is shorter than that of PSS@Tm (1.25 and 6.328 ms, respectively). As shown in Figure S13, (Supporting Information), the parts of the dashed line show the infrared images of the interfingered electrode (IDEs) under different 980 nm light intensities ranging from 0 to 120 mW·cm^{-2}. The results show that no obvious photo-thermal effects were observed on the ceramic base interfingered electrode (IDE) upon 980 nm illumination. Particularly, under 60 mW·cm^{-2} 980 nm illumination, the temperature on the surface of the IDEs is ≈30 °C, revealing that the photo-thermal effect makes no impact on the sensing process.

The gas sensing performances of sensors are generally affected by the activation of adsorbent (O_2, H_2O, etc.) and reaction of activated oxygen species (O_2^-, ·OH, etc.) with target gases on the sensing material surface.[25] **Figure 7** shows the gas sensing mechanism of the "Thylakoid membrane" structural sensor. First, Yb^{3+} as a sensitizer transferred energy to the $^1D_2$ and $^1G_4$ levels of the Tm^{3+} activator to convert NIR light to visible light emission after 980 nm illumination. Second, there are two Routes to produce reactive oxygen species which can react with HCHO. According to Route 1, the high-energy visible photons (Vis) whose energy is higher than the bandgap of AGZO excite the AGZO to generate a photogenerated electron (e^-) -hole (h^+) pair.[48,49] For Route 2, PSS@Tm can transfer energy directly to the AGZO sensing material via non-radiative resonant energy transfer (N-RET).[50] Therefore, the adsorbed oxygen $O_{2\ (abs)}$ on the AGZO surface reacts with these electrons (e^-) to generate O_2^- oxygen species (Formula 1).[16] The adsorbed H_2O on the AGZO surface reacts with the hole (h^+) to generate hydroxyl radical (•OH) (Formula 2).[12,50] Finally, when the HCHO was introduced

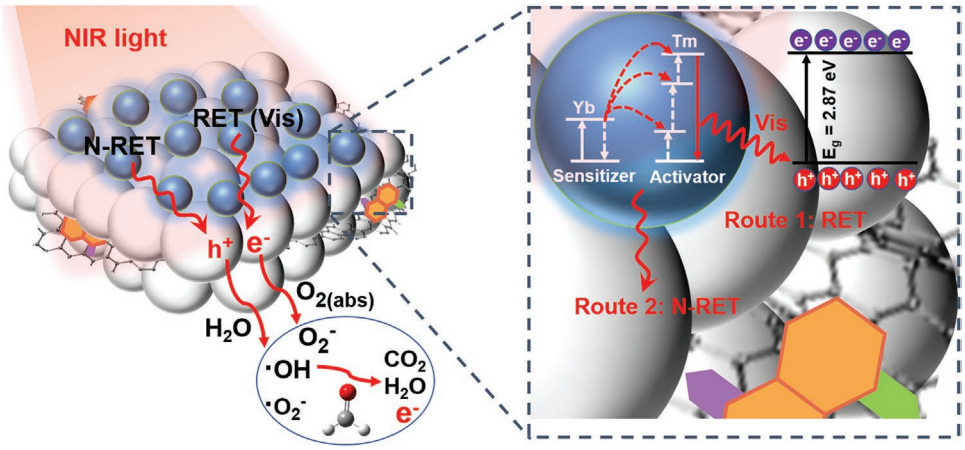

Figure 7. Schematic illustration of the HCHO gas sensing mechanism on AGZO/PSS@Tm "Thylakoid membrane" structural sensor under 980 nm irradiation.

on the AGZO surface, the HCHO react with the O_2^- and ·OH to release the electrons to the AGZO, contributing to the resistance decline of integrated gas sensors (Formula 3 and 4).

$$O_{2(abs)} + e^- (h\nu) \rightarrow O_2^- (\text{Route 1}) \quad (1)$$

$$OH^- + h^+ (h\nu) \rightarrow \bullet OH (h\nu) (\text{Route 2}) \quad (2)$$

$$HCHO + O_2^- (h\nu) \rightarrow CO_2 + H_2O + e^- (\text{Route 1}) \quad (3)$$

$$HCHO + \bullet OH (h\nu) \rightarrow CO_2 + H_2O + 2H^+ + 2e^- (\text{Route 2}) \quad (4)$$

Therefore, the NIR-activated gas sensing process can be realized by constructing a plant-inspired system including UCNPs "light transducer", ANS-rGO "electron transporter" and AGZO "reaction center". In a word, the NIR-mediated HCHO sensing performances of the AGZO/PSS@Tm should derive from the non-radiative/radiative energy transfer (N/RET) from PSS@Tm to AGZO, as well as the NIR-triggered ROS.

3. Conclusion

For the first time, we proposed and demonstrated a universal strategy to construct a plant-inspired light transducer for high-performance NIR-mediated gas sensing at room temperature. Specifically, the use of UCNPs as the "light transducer", ANS-rGO as the "electron transporter", and nanocomposite as the "reaction center" of the "Thylakoid membrane" structural sensor, not only broadens the light adsorption range of the system but also improves the efficiency of internal electron transfer. UCNPs were used for activating gas sensing materials through the non-radiative/radiative energy transfer (N/RET) to realize gas sensing under NIR light. As a model, we employ PSS@Tm to activate AGZO sensing material under 980 nm irradiation to investigate the HCHO sensing properties of AGZO. The as-prepared PSS@Tm can convert 980 nm NIR light to 450 nm blue light, and the upconverted fluorescence spectrum can overlap well with the absorption peak of AGZO. Not surprisingly, AGZO/PSS@Tm-1:50 shows much higher sensitivity under 980 nm irradiation (R_a / R_g = 1.51, 0.4 ppm) than that under direct 450 nm irradiation (R_a / R_g = 1.15, 0.4 ppm) due to the effective energy transfer from PSS@Tm to AGZO and NIR-triggered reactive oxygen species (ROS). The plant-inspired NIR-mediated "Thylakoid membrane" structural sensors have high sensitivity for room temperature formaldehyde detection. More importantly, this work provides a promising alternative to the currently reported UV–vis-activated gas sensors and extended the active wavelength from UV–vis to NIR region. The as-obtained sensors can be further improved to obtain efficient full-spectrum sunlight-activated gas sensors.

4. Experimental Section

Chemicals and Materials: Yttrium acetate ($Y(C_2H_3O_2)_3$, 99.9%), ytterbium acetate ($Yb(C_2H_3O_2)_3$, 99.9%), thulium acetate ($Tm(C_2H_3O_2)_3$, 99.9%), Oleic acid (OA, >90%), 1-octadecene (ODE, >90%), ammonium fluoride (NH_4F, >98%), sodium hydroxide (NaOH, 99%), hydrochloric acid (HCl, ≥37%) and cyclohexane (99.9%) were all purchased from Sigma Aldrich, USA, and used as received. Poly (sodium p-styrenesulfonate) (PSS, Mw: 70 kDa), 5-aminonaphthalene-1-sulfonic acid (ANS, ≥90%), and Zinc nitrate hexahydrate ($Zn(NO_3)_2{\cdot}6H_2O$, 97%) were purchased from Alfa Aesar (Shanghai, P. R. China). The ethanolamine (DEA, 99.9%), ethanol (C_2H_6O, ≥99.7%), and methanol (CH_4O, 99.5%) were obtained from Tianjin Zhiyuan Chemical Reagent Co., Ltd (Tianjin, P. R. China) and used as received without further purification.

Synthesis of OA-coated $NaYF_4$: Yb/Tm (50/2%) and $NaYF_4$: Yb/Er (30/2%) Nanocrystals: The solvent-dispersible Tm^{3+} (2% mol) and Yb^{3+} (50% mol) co-doped $NaYF_4$: Yb/Tm (50/2%) UCNPs were synthesized through the previously reported thermal decomposition method.[3,51] $Y(C_2H_3O_2)_3$ (0.48 mmol), $Yb(C_2H_3O_2)_3$ (0.5 mmol), and $Tm(C_2H_3O_2)_3$ (0.02 mmol) were mixed with 7.5 mL OA and 17.5 mL ODE in a 100 mL flask. The mixture was then heated to 150 °C under stir and then maintained for 1h. After cooling to 70 °C, a 12.5 mL methanol solution containing NaOH (1 mmol) and ammonium fluoride (NH_4F, 10 mmol) was quickly added to the flask and stirred for more than 3 h. The mixture was slowly heated to 100 °C to remove methanol and then heated at 300 °C under Argon protection for 1.5 h. After cooling to ambient temperature, the oleic acid-coated $NaYF_4$: Yb/Tm (50/2%) UCNPs were precipitated with ethanol and washed with ethanol/cyclohexane (2:1 v/v) three times and then dispersed in 8 mL cyclohexane. The oleic acid-capped $NaYF_4$: Yb/Er (30/2%) UCNPs were also obtained in the same manner by the addition of Er^{3+} (2% mol) and Yb^{3+} (30% mol).

Synthesis of PSS-coated $NaYF_4$:Yb/Tm (50/2%) and $NaYF_4$:Yb/Er (30/2%) Nanocrystals: A facile ligand-free method[23] was applied to obtain water-soluble cationic $UCNPs^+$ that can react with anionic PSS^- under water to render the UCNPs water dispersible and negatively charged.[52] Namely, Poly (sodium p-styrenesulfonate) was diluted to 0.2 wt.% using deionized water. The previously obtained UCNPs were treated with HCl solution (pH = 4) under ultrasonic and then washed with deionized water three times to obtain $UCNPs^+$. These ligand-free $UCNPs^+$ were quickly added into the diluted PSS solution and stirred for 1 h. Free PSS was removed by centrifugation at 13000 rpm for 10 min and washed with deionized water three times. Large aggregates were removed using syringe filters (0.22 µm). Finally, the resultant PSS-coated $NaYF_4$: Yb/Tm (50/2%) and $NaYF_4$: Yb/Er (30/2%) could be dispersed in deionized water and labeled as PSS@Tm and PSS@Er, respectively.

Preparation of ANS-functionalized Graphene, Nanocomposites, and Gas Sensors: The graphene oxide (GO) was synthesized by an improved Hummers' method. The 5-aminonaphthalene-1-sulfonic acid-functionalized graphene (ANS-rGO) and ANS-rGO/zinc oxide nanocomposites (AGZO) were prepared by our previous reported technology.[16,53] A spin-coating method was applied in the AGZO/PSS@Tm fabrication. First, 10 µL of AGZO dispersion was spin-coated onto the interdigital electrodes (IDEs, both finger width and gap width are 200 µm) at 3500 rpm for 30 s. Second, 10 µL of PSS@Tm (dilution ratio of 1:10, 1:50, and 1:250) was spin-coated onto the IDEs at 2500 rpm for 30 s. Finally, as-obtained electrodes were dried at 65 °C for 10 min. The AGIn/PSS@Tm, AGSn/PSS@Tm, and AGIn/PSS@Er were also obtained in the same manner. For comparison, 10 µL of PSS@Tm was drop-coated onto the surface of AGZO to obtain AGZO-PSS@Tm-based sensor.

Characterization: The structural and crystallinity of the as-prepared samples were characterized by Fourier transform infrared spectroscopy (FTIR, Vertex 70, Bruker, Germany) and the X-ray diffractometry (XRD, D8 Advance, Bruker, Germany) operated at 45kV using Cu Kα radiation. Atomic force microscope (AFM, Multimode 8, Bruker, USA) was used to measure the thickness and profile of the graphene nanosheets. TEM images of UCNPs and PSS@UCNPs nanocrystals were acquired by transmission electron microscopy (TEM, JEM-2100HR, Japan). The upconversion luminescence spectra and decay curves were detected using a Fluorolog-3 spectrometer (Horiba) equipped with pulsed 980 nm lasers as the excitation source. The UV–vis absorption spectra were measured using a UV–vis spectrophotometer (UV-1750, Shimadzu, Japan). The surface morphologies of as-prepared samples were examined by field emission scanning electron microscopy (FESEM, ZEISS Gemini 500, Germany), in combination with energy dispersive X-ray spectroscopy mapping (EDS mapping). Infrared images were recorded using an infrared thermal camera (PTi120, Fluke).

Gas Sensing Measurements: The sensors were placed in a homemade chamber with temperature and humidity supervision and interior circular systems, as well as a gas inlet and outlet. All the tests were performed at room temperature (30 ± 2 °C) at a relative humidity of 45 ± 3%. Upon exposure to HCHO gas at room temperature under NIR (λ = 980 nm) illumination, the resistance changes of sensors correlated to the surface reaction were recorded by an electrometer (Keithley 2450). The sensing test was monitored under a 980 nm laser (maximum power: 100 mW, FU980AD5-GD16, Shenzhen Fuzhe Technology Co., Ltd.). The light intensity at the sensing materials surface was 60 $mW{\cdot}cm^{-2}$, which was measured by a light intensity meter. The distance between the sensors and the light source had little effect on the light intensity because of the excellent penetration of NIR light. Mathematically, the response (S) is denoted as $S = R_a/R_g$ to HCHO, where R_a and R_g represent the resistance of the sensor in air and the target gases, respectively. The response/recovery times were defined as the time required until 90% of the whole response is reached/recovered.

Supporting Information

Supporting Information is available from the Wiley Online Library or from the author.

Acknowledgements

This work was supported by the National Natural Science Foundation of China (Grant No. 51973070, 62122028, and 11974123), Science and Technology Program of Guangzhou (No. 2019050001), Innovative Team Project of Education Bureau of Guangdong Province (2018KCXTD009), Guangdong Science and Technology Project-International Cooperation (2022A0505050069), Guangdong Basic and Applied Basic Research Foundation (No. 2022A1515010577 and 2018B030306015), Startup Foundation from SCNU, Guangdong Provincial Key Laboratory of Optical Information Materials and Technology (No. 2017B030301007), MOE International Laboratory for Optical Information Technologies, the 111 Project.

Conflict of Interest

The authors declare no conflict of interest.

Data Availability Statement

The data that support the findings of this study are available from the corresponding author upon reasonable request.

Keywords

gas sensors, light transducers, NIR-mediation, thylakoid membranes, upconversion nanoparticles

Received: December 28, 2022
Revised: January 31, 2023
Published online:

[1] H. Tong, S. Ouyang, Y. Bi, N. Umezawa, M. Oshikiri, J. Ye, *Adv. Mater.* **2012**, *24*, 229.
[2] L. Wang, K. G. Gutierrez-Cuevas, H. K. Bisoyi, J. Xiang, G. Singh, R. S. Zola, S. Kumar, O. D. Lavrentovich, A. Urbas, Q. Li, *Chem. Commun.* **2015**, *51*, 15039.
[3] X. Guo, R. Pu, Z. Zhu, S. Qiao, Y. Liang, B. Huang, H. Liu, L. Labrador-Paez, U. Kostiv, P. Zhao, Q. Wu, J. Widengren, Q. Zhan, *Nat. Commun.* **2022**, *13*, 2843.
[4] Q. Zhang, F. Yang, Z. Xu, M. Chaker, D. Ma, *Nanoscale Horizons* **2019**, *4*, 579.
[5] W. L. Wan, B. Tian, Y. J. Lin, C. Korupalli, H. W. Sung, *Nat. Commun.* **2020**, *11*, 534.
[6] B. Gu, Q. Zhang, *Adv. Sci.* **2018**, *5*, 1700609.
[7] R. Chen, J. Wang, Y. Xia, L. Xiang, *Sens. Actuators B Chem.* **2018**, *255*, 2538.
[8] H. Kim, S. Z. Uddin, D. H. Lien, M. Yeh, N. S. Azar, S. Balendhran, T. Kim, N. Gupta, Y. Rho, C. P. Grigoropoulos, K. B. Crozier, A. Javey, *Nature* **2021**, *596*, 232.
[9] C. Hagleitner, A. Hierlemann, D. Lange, A. Kummer, N. Kerness, O. Brand, H. Baltes, *Nature* **2001**, *414*, 293.
[10] J. M. Suh, T. H. Eom, S. H. Cho, T. Kim, H. W. Jang, *Mater. Adv.* **2021**, *2*, 827.
[11] B. N. Shivananju, W. Yu, Y. Liu, Y. Zhang, B. Lin, S. Li, Q. Bao, *Adv. Funct. Mater.* **2016**, *27*, 1603918.
[12] S. Zhang, T. Lei, D. Li, G. Zhang, C. Xie, *Sens. Actuators B Chem.* **2014**, *202*, 964.
[13] S. Y. Jeong, J. S. Kim, J. H. Lee, *Adv. Mater.* **2020**, *32*, 2002075.
[14] Q. Feng, B. Huang, X. Li, *Adv. Funct. Mater.* **2021**, *31*, 2104058.

[15] Z. Li, X. Xu, F. Yu, J. Fei, Q. Li, M. Dong, J. Li, *Angew. Chem.* **2022**, *61*, 16220.
[16] H. Liang, L. Guo, N. Cao, H. Hu, H. Li, N. F. d. Rooij, A. Umar, H. Algarni, Y. Wang, G. Zhou, *J. Mater. Chem. A* **2021**, *9*, 23955.
[17] A. Shanmugasundaram, S. V Manorama, D.-S. Kim, Y.-J. Jeong, D. Weon Lee, *Chem. Eng. J.* **2022**, *448*, 137736.
[18] R. Pu, Q. Zhan, X. Peng, S. Liu, X. Guo, L. Liang, X. Qin, Z. W. Zhao, X. Liu, *Nat. Commun.* **2022**, *13*, 6636.
[19] C. T. Xu, Q. Zhan, H. Liu, G. Somesfalean, J. Qian, S. S. He, S. Andersson-Engels, *Laser and Photonics Reviews* **2013**, *7*, 663.
[20] Q. Zhan, H. Liu, B. Wang, Q. Wu, R. Pu, C. Zhou, B. Huang, X. Peng, H. Agren, S. He, *Nat. Commun.* **2017**, *8*, 1058.
[21] B. Zhou, B. Shi, D. Jin, X. Liu, *Nat. Nanotechnol.* **2015**, *10*, 924.
[22] J. Ma, Y. Li, J. Li, X. Yang, Y. Ren, A. A. Alghamdi, G. Song, K. Yuan, Y. Deng, *Adv. Funct. Mater.* **2021**, *32*, 2107439.
[23] N. Bogdan, F. Vetrone, G. A. Ozin, J. A. Capobianco, *Nano Lett.* **2011**, *11*, 835.
[24] J. Jin, Y. J. Gu, C. W. Man, J. Cheng, Z. Xu, Y. Zhang, H. Wang, V. H. Lee, S. H. Cheng, W. T. Wong, *ACS Nano* **2011**, *5*, 7838.
[25] K. Hagedorn, W. Li, Q. Liang, S. Dilger, M. Noebels, M. R. Wagner, J. S. Reparaz, A. Dollinger, J. S. a. d. Günne, T. Dekorsy, L. Schmidt-Mende, S. Polarz, *Adv. Funct. Mater.* **2016**, *26*, 3424.
[26] R. Kim, J. S. Jang, D. H. Kim, J. Y. Kang, H. J. Cho, Y. J. Jeong, I. D. Kim, *Adv. Funct. Mater.* **2019**, *29*, 1903128.
[27] C. Zheng, M. Yin, R. Ge, J. Wei, B. Su, X. Chen, X. Chen, *Biosens. Bioelectron.* **2021**, *185*, 113278.
[28] Z. Wang, B. Liu, Q. Sun, L. Feng, F. He, P. Yang, S. Gai, Z. Quan, J. Lin, *ACS Nano* **2021**, *15*, 12342.
[29] A. A. Ansari, M. Sillanpää, *Renew. Sust. Energ. Rev.* **2021**, *151*, 111631.
[30] Y. Tang, W. Di, X. Zhai, R. Yang, W. Qin, *ACS Catal.* **2013**, *3*, 405.
[31] C. Yao, W. Wang, P. Wang, M. Zhao, X. Li, F. Zhang, *Adv. Mater.* **2018**, *30*, 1704833.
[32] Q. Tian, W. Yao, Z. Wu, J. Liu, L. Liu, W. Wu, C. Jiang, *J. Mater. Chem. A* **2017**, *5*, 23566.
[33] Y. Liu, S. Cheng, S. Zhan, X. Wu, *Inorg. Chem.* **2021**, *6*, 5704.
[34] F. Zhou, B. Zheng, Y. Zhang, Y. Wu, H. Wang, J. Chang, *Nanotechnology* **2016**, *27*, 235601.
[35] D. Zhang, Y. Cao, Z. Yang, J. Wu, *ACS Appl. Mat. Inter.* **2020**, *12*, 11979.
[36] J. Fan, H. Li, H. Hu, Y. Niu, R. Hao, A. Umar, M. S. Al-Assiri, M. A. Alsaiari, Y. Wang, *Microchem. J.* **2021**, *160*, 105607.
[37] H. Hu, H. Liang, J. Fan, L. Guo, H. Li, N. F. de Rooij, A. Umar, H. Algarni, Y. Wang, G. Zhou, *ACS Appl. Mat. Inter.* **2022**, *14*, 13186.
[38] J. Tian, X. Chen, T. Wang, W. Pei, F. Li, D. Li, Y. Yang, X. Dong, *Sens. Actuators B Chem.* **2021**, *344*, 130227.
[39] P. Wang, X. Zou, H. Tan, S. Wu, L. Jiang, G. Zhu, *J. Mater. Chem. C* **2018**, *6*, 5412.
[40] W. Ling, D. Zhu, Y. Pu, H. Li, *Sens. Actuators B Chem.* **2022**, *355*, 131294.
[41] Y. K. Jo, S. Y. Jeong, Y. K. Moon, Y. M. Jo, J. W. Yoon, J. H. Lee, *Nat. Commun.* **2021**, *12*, 4955.
[42] Y. Wang, Y. Zhou, Y. Wang, *Sens. Actuators B Chem.* **2020**, *323*, 128695.
[43] Q. Lyu, S. Gong, J. G. Lees, J. Yin, L. W. Yap, A. M. Kong, Q. Shi, R. Fu, Q. Zhu, A. Dyer, J. M. Dyson, S. Y. Lim, W. Cheng, *Nat. Commun.* **2022**, *13*, 7259.
[44] W. Wang, M. Zhao, C. Zhang, H. Qian, *Chem. Rec.* **2020**, *20*, 2.
[45] T. Cheng, R. O'Rorke, R. F. Ortiz, T. Y. Yan, E. Hemmer, F. Vetrone, R. S. Marks, T. W. J. Steele, *Acta Biomater.* **2017**, *54*, 186.
[46] D. Mendez-Gonzalez, O. G. Calderon, S. Melle, J. Gonzalez-Izquierdo, L. Banares, D. Lopez-Diaz, M. M. Velazquez, E. Lopez-Cabarcos, J. Rubio-Retama, M. Laurenti, *J. Colloid Interface Sci.* **2020**, *575*, 119.
[47] T D. Tu, L. Liu, Q. Ju, Y. Liu, H. Zhu, R. Li, X. Chen, *Angew. Chem.* **2011**, *50*, 6306.
[48] F. Wang, R. Deng, J. Wang, Q. Wang, Y. Han, H. Zhu, X. Chen, X. Liu, *Nat. Mater.* **2011**, *10*, 968.
[49] X. Guo, W. Song, C. Chen, W. Di, W. Qin, *Phys. Chem. Chem. Phys.* **2013**, *15*, 14681.
[50] W.-N. Wang, C.-X. Huang, C.-Y. Zhang, M.-L. Zhao, J. Zhang, H.-J. Chen, Z.-B. Zha, T. Zhao, H.-S. Qian, *Applied Catalysis, B* **2018**, *224*, 854.
[51] Y. Liang, Z. Zhu, S. Qiao, X. Guo, R. Pu, H. Tang, H. Liu, H. Dong, T. Peng, L. D. Sun, J. Widengren, Q. Zhan, *Nat. Nanotechnol.* **2022**, *17*, 524.
[52] N. Estebanez, M. Gonzalez-Bejar, J. Perez-Prieto, *ACS Omega* **2019**, *4*, 3012.
[53] Z. Chen, J. Wang, D. Pan, Y. Wang, R. Noetzel, H. Li, P. Xie, W. Pei, A. Umar, L. Jiang, N. Li, N. F. Rooij, G. Zhou, *ACS Nano* **2018**, *12*, 2521.